Primljen / Received: 13.4.2025.
Ispravljen / Corrected: 27.7.2025.
Prihvaćen / Accepted: 30.8.2025.
Dostupno online / Available online: 10.11.2025.

Experimental study on seismic performance of adaptive damper

Authors:

[1]Xiaowei Yang, PhD. CE
yxw43@163.com
Corresponding author

[1]Yiqiong Zhang, MSc. CE
z0611yq@163.com

[2]Prof. Kaihai Luo, PhD. CE
nile-fisher@hotmail.com

[1]Cong Zhao, MSc. CE
lmy3977@163.com

[1]Mengyuan Li, MSc. CE
z7613c@163.com

[1] Zhongyuan University of Technology, China
School of Intelligent Building and Civil Engineering
[2] China Academy of Civil Engineering Research, Beijing, China
Institute of Earthquake Engineering Research

Research Paper

Xiaowei Yang, Yiqiong Zhang, Kaihai Luo, Cong Zhao, Mengyuan Li

Experimental study on seismic performance of adaptive damper

To address the challenges of irreversible structural plastic deformation in traditional building seismic designs and the significant stiffness degradation of existing metal dampers, this study proposes an adaptive damper support based on multistage X-shaped steel plate bending deformation. By implementing a contact mechanism, the proposed adaptive damper enables the coordinated energy dissipation of X-shaped steel plates at different stages, thereby achieving stiffness superposition and staged yielding. Using low-cycle repeated pseudo-static tests and finite element numerical simulations, the hysteretic characteristics, stiffness degradation patterns, and energy dissipation capacities of the specimens were systematically investigated. The results demonstrate that as the displacement increases, the adaptive damper sequentially activates multi-stage energy-dissipating units, with the hysteretic curve exhibiting multi-peak characteristics. The equivalent viscous damping coefficient shows stage-wise fluctuations with increasing displacement. Further, the stiffness degradation process is triggered by the contact mechanism, and follows an alternating evolution pattern of degradation and enhancement to effectively balance the requirements for energy dissipation and stiffness retention. This study provides a theoretical basis for a novel adaptive energy-dissipating device for structural seismic designs.

Key words:
adaptive damper, multi-step energy dissipation, stiffness superposition, seismic performance

Prethodno priopćenje

Xiaowei Yang, Yiqiong Zhang, Kaihai Luo, Cong Zhao, Mengyuan Li

Eksperimentalno istraživanje seizmičkog ponašanja adaptivnih prigušivača

Kako bi se odgovorilo na izazove ireverzibilne plastične deformacije konstrukcija pri tradicionalnome projektiranju potresne otpornosti zgrada i znatnog smanjenja krutosti postojećih metalnih prigušivača, u ovome se radu predlaže adaptivni prigušivač s osloncem, temeljen na višestupanjskoj deformaciji uzrokovanoj savijanjem čelične ploče u obliku slova "X". Uvođenjem mehanizma kontakta predloženi adaptivni prigušivači omogućuju usklađeno trošenje energije čeličnih ploča u obliku slova "X" u različitim fazama, čime se postižu superpozicija krutosti i postupno popuštanje. Primjenom niskocikličkih ponovljenih pseudostatičkih ispitivanja i numeričkih simulacija konačnih elemenata sustavno su ispitana histerezna svojstva, obrasci smanjenja krutosti i kapaciteti trošenja energije uzoraka. Iz rezultata ispitivanja vidljivo je da s povećanjem pomaka adaptivni prigušivač uzastopno aktivira višestupanjske jedinice za trošenje energije, pri čemu histerezna krivulja pokazuje karakteristike više vrhova. Ekvivalentni koeficijent viskoznog prigušenja pokazuje stupnjevite promjene s povećanjem pomaka. Osim toga proces smanjenja krutosti uzrokovan je kontaktnim mehanizmom i slijedi naizmjenični razvoj obrazaca degradacije i poboljšanja kako bi se učinkovito uravnotežili zahtjevi za trošenjem energije i zadržavanjem krutosti. Ovo istraživanje pruža teorijsku osnovu za novi adaptivni uređaj za trošenje energije za projektiranje potresne otpornosti konstrukcija.

Ključne riječi:
adaptivni prigušivač, višestupanjsko trošenje energije, superpozicija krutosti, seizmičko ponašanje

1. Introduction

Load-bearing capacity and deformation mechanism of traditional building structures enable them to withstand seismic forces. However, substantial residual deformation and component damage may occur as a result of severe earthquakes, posing significant challenges for post-earthquake recovery and reconstruction. These issues have been addressed in previous research [1, 2], with some studies demonstrating significant mitigation of structural damage through the application of energy dissipation and vibration control technologies [3, 4]. These technologies employ strategically placed damping devices to absorb seismic energy and reduce the dynamic response of the structure. Following the pioneering design concept of metal buckling dampers, substantial advancements have been made [5], including the development of various metal buckling dampers, which optimise performance and expand engineering applications, while also establishing a solid foundation for further technological advancements [6-9].

Metal-bending yield dampers are widely utilised owing to their exceptional ductility and robust energy dissipation capabilities [10-13]. These devices, particularly triangular and X-shaped steel plate dampers, have been studied extensively [14-19], and have been demonstrated to achieve an even stress distribution across sections through out-of-plane bending forces, thereby enhancing energy dissipation. However, these dampers predominantly exhibit single-order energy-dissipation characteristics, providing an initial stiffness which rapidly decreases post-yielding, potentially leading to significant residual deformations under sustained external forces.

To overcome the limitations of single-stage dampers, dual-stage composite dampers have been introduced, which can effectively mitigate the plastic deformation under various seismic intensities. Innovations in this area include a two-stage energy dissipation system [20] consisting of a plate friction damper connected to an H-shaped steel beam, two-stage buckling constraint support [21], radial contact series concentric short steel pipe buckling dampers [22], ring-graded yield metal dampers [23], and two-stage yield metal restraint support [24]. Although these designs improve stiffness attenuation during the energy dissipation process, the stiffness may still decrease after the second stage, resulting in significant residual deformation following rare and extremely rare earthquakes. Consequently, the development of new multistage buckling metal dampers is crucial for providing multi-tiered protection to the main structure under varying earthquake intensities.

Recent studies on the application of energy-dissipation devices in bridges and buildings have further solidified the practical foundations of this technology. Ristic et al. [25] and Ristic et al. [26] conducted seismic experiments on isolated bridge models enhanced with novel V-gapped and uniform-gapped HS devices, respectively, thereby confirming the effectiveness of these devices in reducing seismic damage to bridges. Zhang et al. [27] explored the seismic dissipation mechanisms of interstory isolation structures and provided a theoretical basis for optimising the isolation system performance. Dang et al. [28] investigated the design methods and engineering applications of shear walls equipped with friction energy dissipation dampers, highlighting the practical potential of friction-based energy dissipation devices in building structures.

In this study, we propose an adaptive damper support system as shown in Figures 1 and 2. To address the limitations of two-stage composite dampers, our adaptive dampers feature three stages of energy dissipation using X-shaped steel plates as energy-dissipating components combined with three distinct contact devices. During the initial small axial deformations, X-shaped steel plate 1 engaged in energy dissipation through bending deformation. As the axial displacement increased, the contact mechanism activated the bending deformation in the X-shaped steel plate 2, initiating stiffness accumulation and further energy dissipation. The continued axial deformation caused X-shaped steel plate 3 to enter its energy-dissipation state through a similar mechanism, resulting in additional stiffness accumulation. The design of the damping device allows it to adapt to displacement variations while effectively dissipating energy and enhancing the stiffness.

This study provides a comprehensive description of the damper structure and operational principles. Further, an evaluation and comparison of the stiffness and energy dissipation characteristics of three different energy-dissipating specimens are presented through low-cycle reciprocating pseudostatic experiments and finite element numerical simulations.

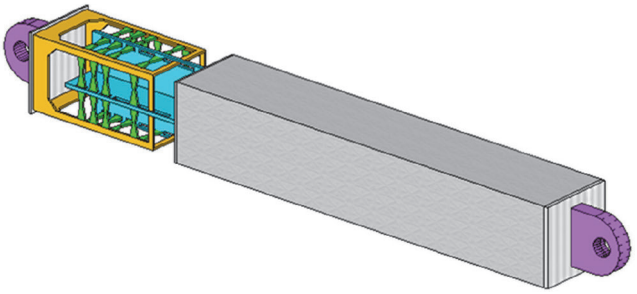

Figure 1. Schematic diagram of the adaptive damper support

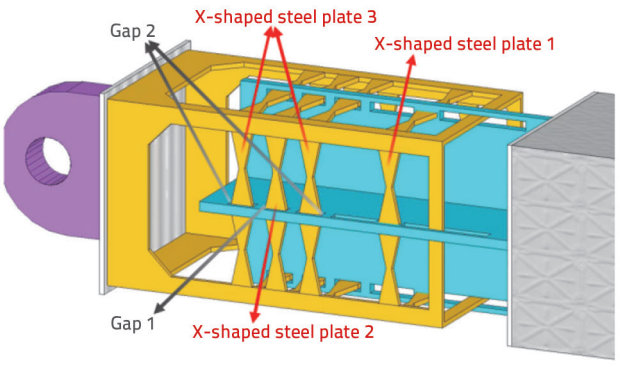

Figure 2. Schematic diagram of the energy consumption component

2. Adaptive dampers: construction and operating principles

2.1. Construction of dampers

Based on structural symmetry, a unilateral energy-dissipating component was selected and its stiffness and energy-dissipation characteristics were investigated experimentally. Its structure is illustrated in Figure 3. Energy dissipation is mainly achieved through the bending and deformation of the X-shaped steel plate. In the central steel plate, gaps are reserved according to the position of the X-shaped steel plate to realise the functions of the second- and third-order energy consumption and stiffness superposition.

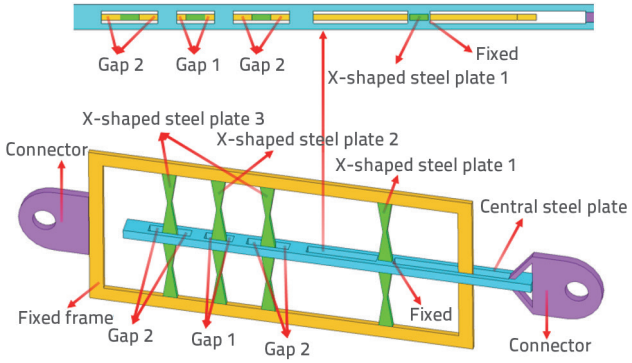

Figure 3. Adaptive damper structure diagram

2.2. Operating principle of dampers

The operational process of the X-shaped steel plates within the adaptive damper can be categorised into two distinct stages: the elastic and yield-strengthening stages. The energy dissipation process of the entire damper is segmented into three stages, and schematic diagrams illustrating the deformation at each energy dissipation stage are presented in Figure 4–6. Focusing on a single loading direction, the operational process of the adaptive damper is analysed as follows:

- As depicted in Figure 4, in the first energy dissipation stage, when the central steel plate undergoes a minor axial displacement under the action of external forces, fixed X-shaped steel plate 1 enters the elastoplastic deformation state to achieve energy dissipation. The other X-shaped steel plates remained stationary because of the gap.
- As shown in Figure 5, during the second energy-dissipation stage, as the displacement of the central steel plate increases, the constraints imposed by the holes and gaps in the central steel plate activate the contact mechanism at gap 1. Consequently, X-shaped steel plate 2, located at gap 1, together with X-shaped steel plate 1, undergoes elastic-plastic deformation, facilitating energy dissipation. This coordinated deformation results in enhanced stiffness of the energy dissipation component.

As illustrated in Figure 6, in the third energy-dissipation stage, when the displacement of the central steel plate continued to increase, the contact mechanism at gap 2 was triggered. X-shaped steel plate 3 at gap 2 begins to deform and jointly undergoes elastoplastic deformation and energy dissipation with X-shaped steel plates 1 and 2 at gap 1. The damping force further increased, and the stiffness continued to increase, effectively preventing a reduction in the stiffness of the damper.

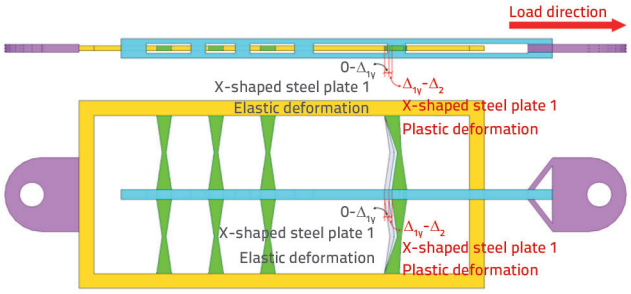

Figure 4. Initial stage of damper operation

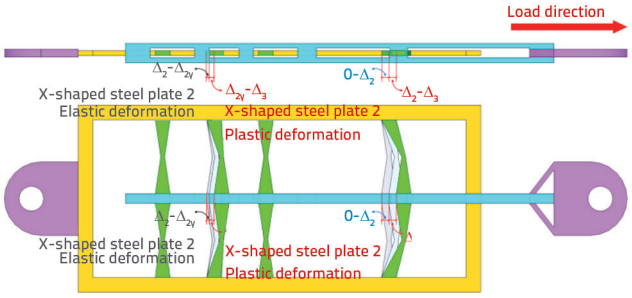

Figure 5. Engagement of second-order dampers in the operational phase

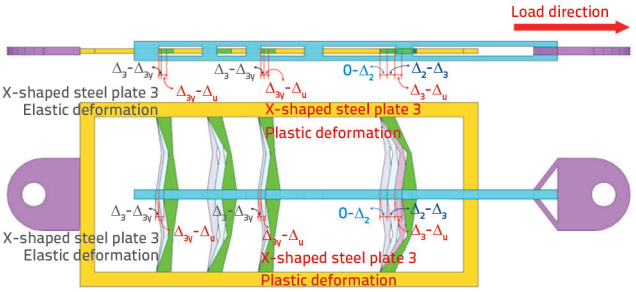

Figure 6. Involvement of third-order dampers in the operational stage

3. Specimen design and experiment

3.1. Specimen design

To investigate the stiffness and energy dissipation performance of the adaptive damper supporting member under low-cycle reciprocating pseudostatic loading, an adaptive damper specimen was fabricated, as shown in Figure 7. For comparative experiments, first- and second-order dampers were designed as illustrated in Figures 8 and 9, respectively. The primary difference between the three dampers lies in the configuration of the X-shaped steel plates; all other structural components remain identical. The thicknesses of both the outer steel frame and X-shaped steel plates were 10 mm, while the effective spacings of gaps 1 and 2 were 2 and 4 mm, respectively.

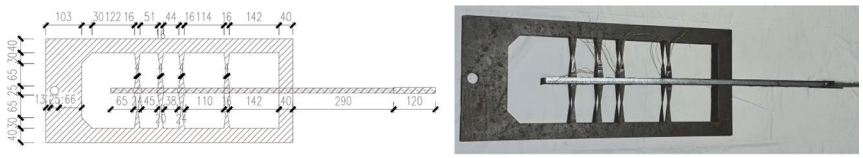

Figure 7. Adaptive damper (D-3) size and physical diagram

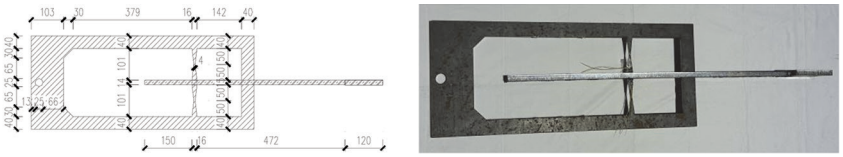

Figure 8. First-order damper (D-1) size and physical diagram

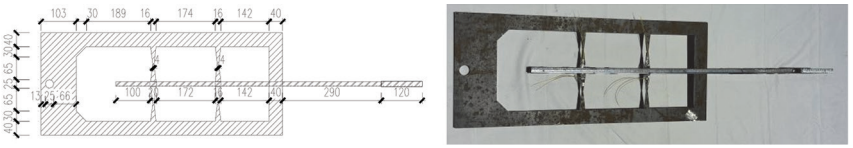

Figure 9. Two-stage damper (D-2) size and physical diagram

Figure 10. Specimen steel plate

3.2. Material mechanical property test

Q235 steel was selected for the test specimens. To ascertain its precise mechanical properties [29], two steel plates were randomly selected from the base material for sample fabrication (Figures 10 and 11). Subsequently, the mechanical properties of the samples were tested. The stress-strain curve derived from the test is shown in Figure 12. The mechanical properties of the materials are listed in Table 1.

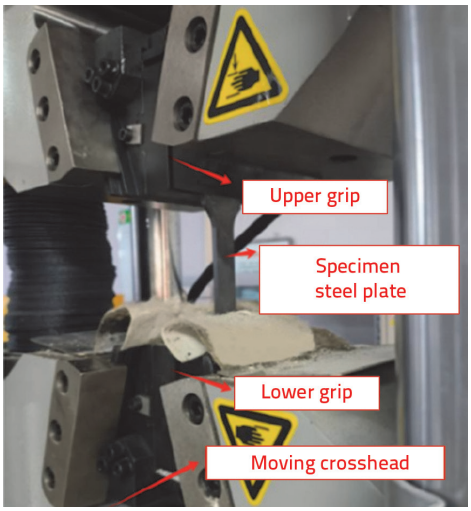

Figure 11. Standard tensile experiment to determine the mechanical properties of steel

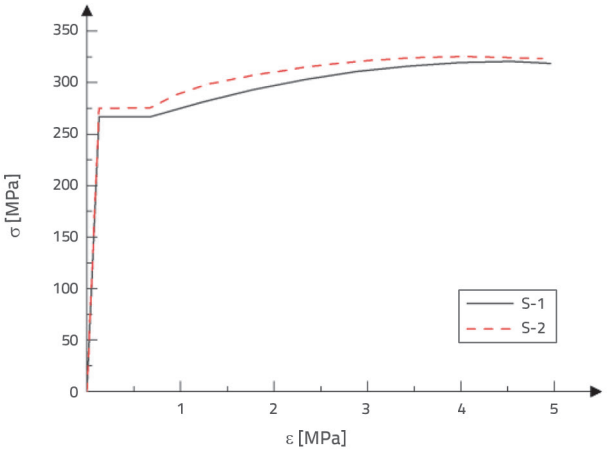

Figure 12. Stress-strain relationship of steel

3.3. Experimental apparatus and loading system

The loading device is shown in Fig. 13. A low-cycle reciprocating pseudostatic experiment was performed on the experimental piece using the displacement loading system shown in Figure 14. The experimental conditions are shown in Figure 15.

Table 1. Material properties of steel

Sample	f_y [MPa]	f_u [MPa]	E_s [N/mm^2]	ν
S-1	271	320	2,04×105	0.3
S-2	275	325	2,10×105	0.3
Average value	273	322,5	2,07×105	0.3

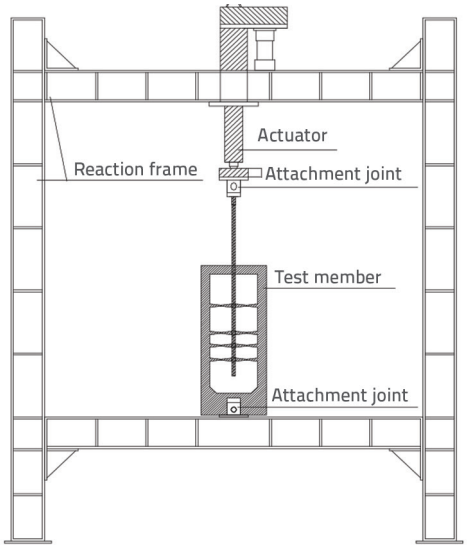

Figure 13. Loading device

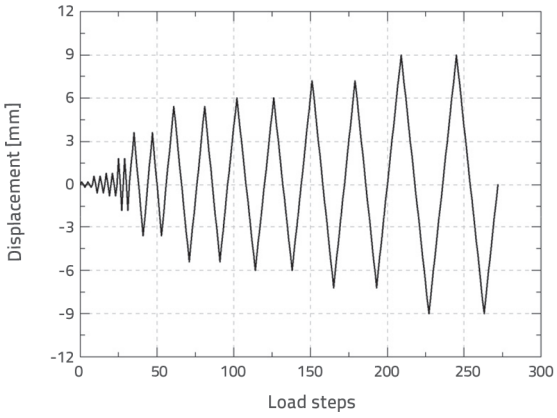

Figure 14. Loading system

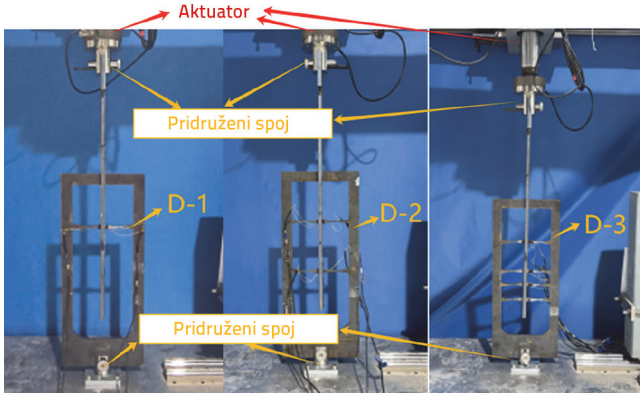

Figure 15. D - 1, D - 2 and D - 3 experiment

4. Adaptive dampers: construction and operating principles

4.1. Hysteretic curves of specimen experiment

The force-displacement hysteresis curves obtained from the damper component experiments are shown in Figure 16. The hysteresis curve exhibited well-developed bilinear characteristics for specimen D-1, demonstrated two-stage energy dissipation behaviour for specimen D-2, and showed remarkable multistage energy dissipation effects for specimen D-3.

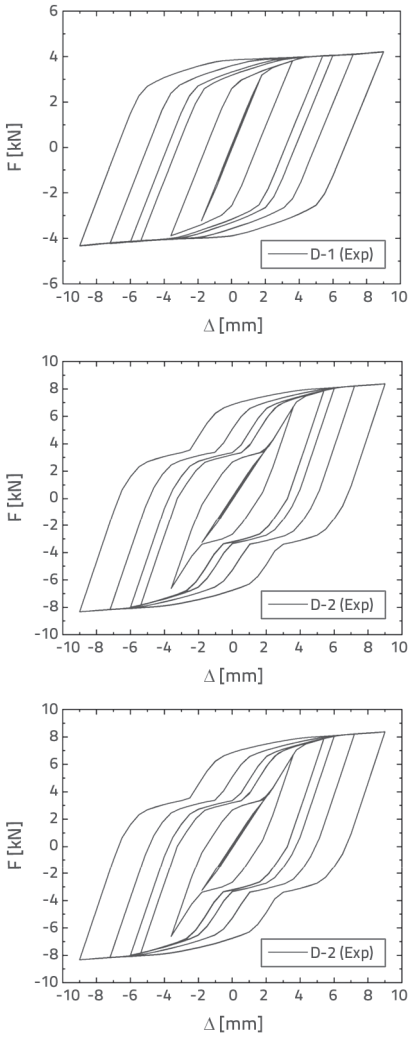

Figure 16. Hysteretic curve of specimen experiment

This phenomenon occurs because as the axial displacement of the central steel plate increases under external loading and X-shaped steel plate 1 yields, the motion of the central steel plate is restricted by its contact gap and the contact mechanism is activated at gap 1. At this stage, X-shaped steel plate 2 interacts with the fixed X-shaped steel plate 1, thereby increasing the damping force and stiffness. As X-shaped steel plate 2 undergoes elastoplastic deformation and participates in the combined energy dissipation, the area enclosed by the hysteresis loop expands, further enhancing the energy dissipation capacity. With further increases in the external loading, the displacement of the central steel plate continues to increase, triggering the contact mechanism at gap 2. Here, X-shaped steel plate 3 interacts with X-shaped steel plates 2 and 1, increasing the damping force and stiffness. The elastoplastic deformation of the X-shaped steel plate 3 similarly

promotes its participation in the combined energy dissipation, further increasing the area enclosed by the hysteresis loop and enhancing the energy dissipation capacity. This sequential activation of the X-shaped steel plates enabled the damper to exhibit the adaptive characteristics of staged yielding and multistage energy dissipation.

4.2. Skeleton line of specimen experiment

The skeleton curves obtained from the damper component experiments are shown in Figure 17. The skeleton curve of specimen D-1 exhibits approximately bilinear elastic-plastic characteristics. The skeleton curve of specimen D-2 demonstrates a two-stage behaviour: as the displacement of the central steel plate increases, the damping force strengthens, and the stiffness undergoes a single elevation. The skeleton curve of specimen D-3 displayed the expected three-stage characteristics: with a further increase in the displacement of the central steel plate, the damping force continued to strengthen, and the stiffness experienced two increments, manifesting superior adaptive capabilities.

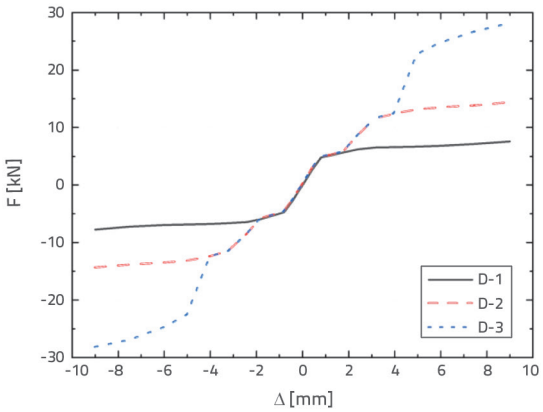

Figure 17. Skeleton line of the specimen

4.3. Stiffness degradation curve of specimen experiment

The specimen stiffness can be represented by the secant stiffness, and the secant stiffness k_i is calculated according to Eqn. (1)(JGJ101-2015) [29]:

$$k_i = \frac{|+F_i| + |-F_i|}{|+\Delta_i| + |-\Delta_i|} \tag{1}$$

Here, $+F_i$, $-F_i$ are the load values at the i th positive and reverse peak points; $+\Delta_i$, $-\Delta_i$ are the displacement values at the i th positive and reverse peak points.

The stiffness degradation curves of the damper specimens are presented in Figure 18. As the displacement of the central steel plate increased, the stiffness degradation trends of the three specimens remained consistent before the activation of the contact mechanism. However, with further displacement of the central steel plate, Specimen D-1, which was equipped with only a single X-shaped steel plate as its energy-dissipating component, exhibited continuous stiffness degradation after energy dissipation. For Specimen D-2, the activation of the contact mechanism triggered X-shaped steel plate 2 at gap 1, which subsequently cooperated with X-shaped steel plate 1. This interaction enhances the damping force and induces an initial stiffness recovery, resulting in a stiffness trend characterised by initial degradation followed by enhancement. Specimen D-3, which was outfitted with two contact mechanisms, sequentially activated the contact mechanisms at gaps 1 and 2 as the displacement of the central steel plate increased, successively activating X-shaped steel plates 2 and 3 to cooperate with the fixed X-shaped steel plate 1. Notably, when X-shaped steel plate 3 was activated, the damping force increased significantly, and the stiffness underwent a complex transformation of the initial degradation, followed by enhancement. Ultimately, this process achieved two stiffness enhancements, demonstrating its superior adaptability.

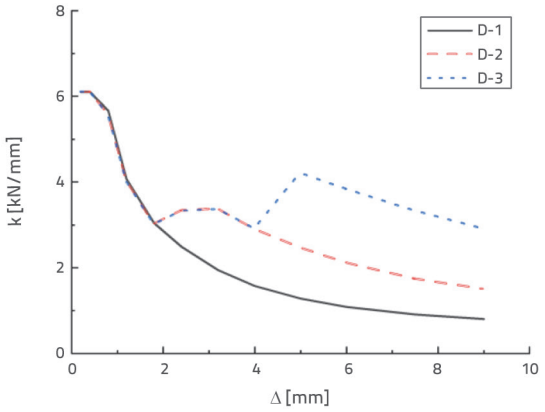

Figure 18. Skeleton line of the specimen

4.4. Energy dissipation capacity of specimen experiment

The energy dissipation capacity of the specimen can be determined by the area enclosed by the analytical load - deformation hysteretic curve (JGJ101-2015) [29]. This index is usually evaluated using the equivalent viscous damping coefficient ζ, and Eqn. (2) is as follows:

$$\varsigma = \frac{1}{2\pi} \cdot \frac{S_{(\Delta ABC+\Delta CDA)}}{S_{(\Delta OBE+\Delta ODF)}} \tag{2}$$

Here, $S_{(\Delta ABC+\Delta CDA)}$-the area enclosed by the hysteresis curve in Figure 21; $S_{(\Delta OBE+\Delta ODF)}$ -the sum of the areas of triangle OBE and triangle ODF in Figure 19.

As shown in Figure 20, with the increase of the central steel plate's displacement, the equivalent viscous damping coefficient ζ of Specimen D-1 rapidly reaches a steady state after the X-shaped steel plate 1 undergoes elastic-plastic deformation, ultimately reaching 50 % at the maximum displacement of the test loading. For Specimen D-2, its

equivalent viscous damping coefficient ζ first increases rapidly and then slightly declines. This is because the X-shaped steel plate 2 only underwent elastic deformation when first engaged, and failed to dissipate energy effectively, thereby reducing the area enclosed by the hysteresis loop. Once it transitions into elastic-plastic deformation, ζ increases again to 44.3 %. A similar trend is observed for Specimen D-3: ζ initially increases rapidly but declines slightly as X-shaped steel plate 2, in its early engagement phase, experiences only elastic deformation. As the central steel plate's displacement further increases, X-shaped steel plate 2 enters elastic-plastic deformation, causing ζ to increase again. However, ζ then decreases when X-shaped steel plate 3, upon initial engagement, undergoes elastic deformation. Only after X-shaped steel plate 3 also transitions into elastic-plastic deformation does ζ increase sharply, eventually stabilising at 34 %.

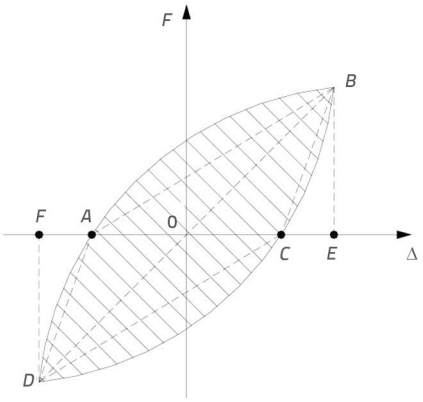

Figure 19. Curve hysteresis loop

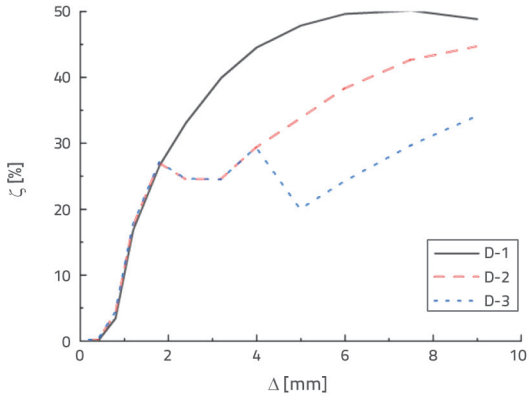

Figure 20. Equivalent viscous damping coefficient ζ curves

These findings indicate that, in multistage dampers with series-connected contact-type X-shaped steel plates, the X-shaped steel plates activated by the contact mechanism exhibit insufficient energy dissipation capacity during their elastic deformation phase. Consequently, when the displacement exceeded the yield displacement of a single-stage X-shaped steel plate damper, the energy-dissipation performance was inferior to that of the single-stage X-shaped steel plate buckling dampers.

5. Damper finite element simulation experiments

5.1. Finite element modelling

To investigate the seismic performance characteristics of this type of damper comprehensively, a research methodology integrating component testing with finite element method (FEM) numerical simulations was adopted. This approach analysed the influence patterns of X-shaped steel plates with varying dimensions (Figure 21, Table 2) and contact gaps of different sizes (Figure 22, Table 3) on the seismic performance of the damper, leading to the construction of a total of 25 FEA models. As illustrated in Figures 23–25, based on the material test data and design parameters, the FEA models were discretised using hexahedral solid elements of type 7. The components on both sides of the contact gaps were defined as contact bodies. Three-directional translational constraints were applied to the left side of the frame, and a synchronous reciprocating load application was achieved through connection elements at the right loading end of the middle steel plate. Q235-grade steel was selected, with material properties specified as: elastic modulus E=206 GPa, Poisson's ratio ν=0.3, and yield strength f_y=273 MPa. The constitutive relationship adopted an elastoplastic bilinear hardening model with a hardening coefficient of 1.3. A comparison of the hysteresis curves from the experimental and numerical simulations (Figure 26) exhibited good consistency, thereby validating the effectiveness of the FEA approach in simulating the damper performance.

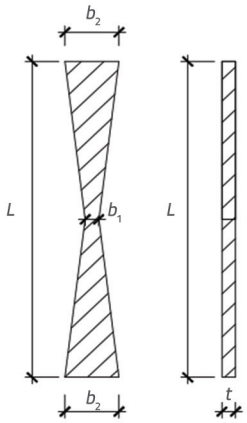

Figure 21. Schematic diagram of the size parameters of X-type steel plate

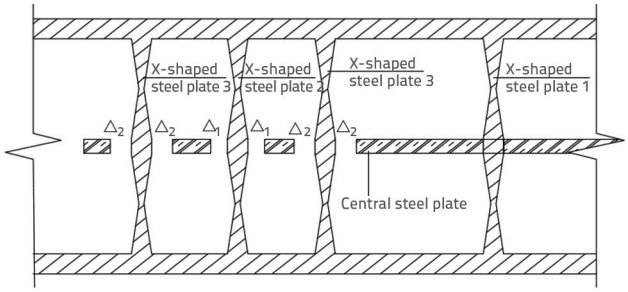

Figure 22. Schematic diagram of contact gap

Table 2. Influence of X-Plate size

Model number		X-Plate size [mm]										F_{2y} / F_{1y}	F_{3y} / F_{2y}
		b_1	b_2	b_1	b_2	b_1	b_2	t	L	Δ_1	Δ_2		
Group D-1F	D-1FA	4	12	-	-	-	-	10	50	-	-	-	-
	D-1FB	4	14	-	-	-	-	10	50	-	-	-	-
	D-1FC	4	16	-	-	-	-	10	50	-	-	-	-
	D-1FD	4	18	-	-	-	-	10	50	-	-	-	-
	D-1FE	4	20	-	-	-	-	10	50	-	-	-	-
Group D-2F	D-2FA	4	16	4	12	-	-	10	50	3	-	0.66	-
	D-2FB	4	16	4	14	-	-	10	50	3	-	0.80	-
	D-2FC	4	16	4	16	-	-	10	50	3	-	1	-
	D-2FD	4	16	4	18	-	-	10	50	3	-	1.07	-
	D-2FE	4	16	4	20	-	-	10	50	3	-	1.21	-
Group D-3F	D-3FA	4	16	4	16	4	12	10	50	3	6	1	1.32
	D-3FB	4	16	4	16	4	14	10	50	3	6	1	1.60
	D-3FC	4	16	4	16	4	16	10	50	3	6	1	2
	D-3FD	4	16	4	16	4	18	10	50	3	6	1	2.15
	D-3FE	4	16	4	16	4	20	10	50	3	6	1	2.42

Table 3. Influence of contact gaps

Model number		X-Plate size [mm]										Δ_1 /Δ_{1y}	Δ_2 /Δ_{2y}
		b_1	b_2	b_1	b_2	b_1	b_2	t	L	Δ_1 (Gap 1)	Δ_2 (Gap 2)		
Group D-2	D-2A	4	16	4	16	-	-	10	50	1	-	0.5	-
	D-2B	4	16	4	16	-	-	10	50	2	-	1	-
	D-2C	4	16	4	16	-	-	10	50	3	-	1.5	-
	D-2D	4	16	4	16	-	-	10	50	4	-	2	-
	D-2E	4	16	4	16	-	-	10	50	5	-	2.5	-
Group D-3	D-3A	4	16	4	16	4	16	10	50	3	4	1.5	2
	D-3B	4	16	4	16	4	16	10	50	3	5	1.5	2.5
	D-3C	4	16	4	16	4	16	10	50	3	6	1.5	3
	D-3D	4	16	4	16	4	16	10	50	3	7	1.5	3.5
	D-3E	4	16	4	16	4	16	10	50	3	8	1.5	4

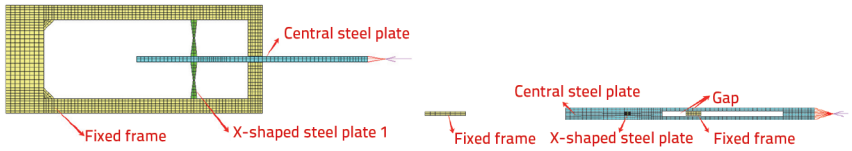

Figure 23. D-1 finite element model

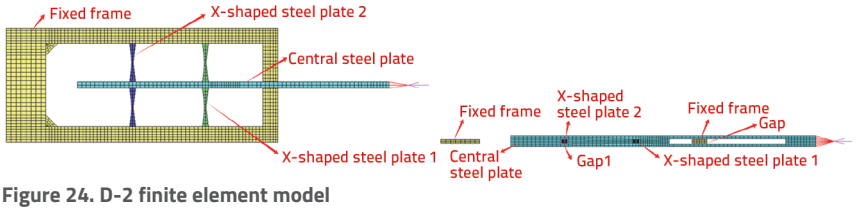

Figure 24. D-2 finite element model

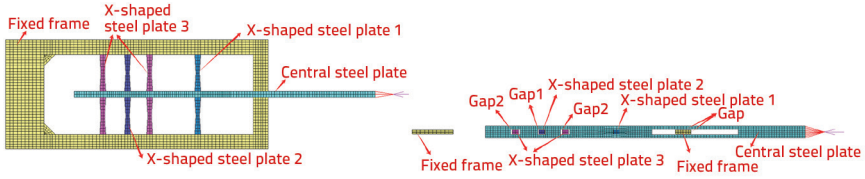

Figure 25. D-3 finite element model

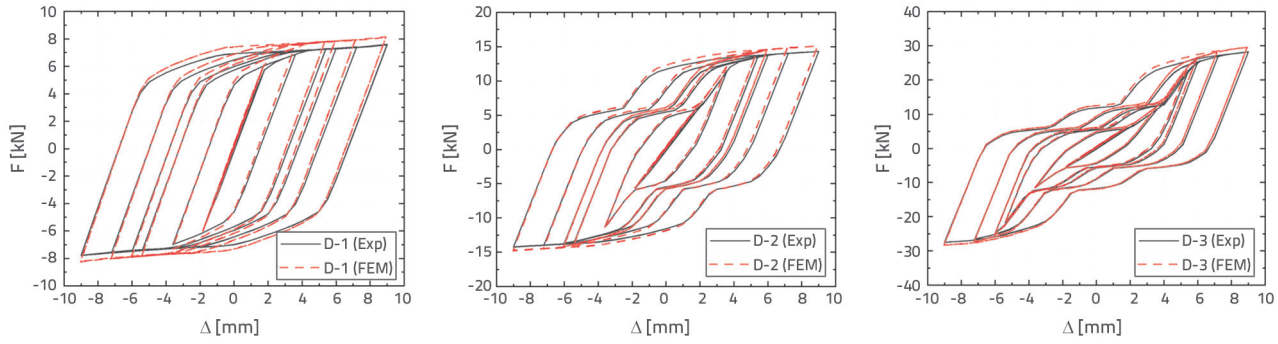

Figure 26. Comparison of FEM simulation and test results

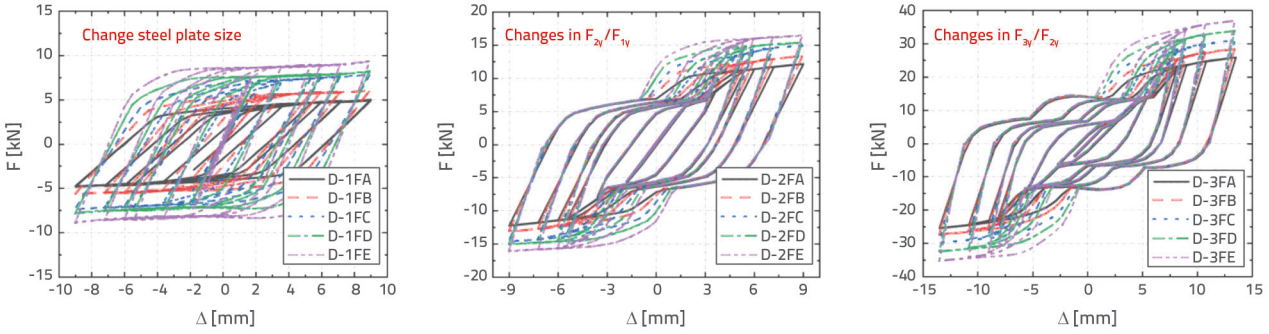

Figure 27. Hysteretic curve with changes in damper size

5.2. Hysteretic curve

The hysteresis curves for dampers with varying dimensions are shown in Figure 27. For Group D-1F, the hysteresis curves exhibit distinct bilinear characteristics, with the enclosed area of the curve expanding as the dimensions of the X-shaped steel plates increase. In contrast, the curves of Groups D-2F and D-3F display multi-stage features. Specifically, within Group D-2F, when modifying the dimensions of X-shaped steel plate 2, the enclosed area of the second stage in the hysteresis curve increased as the F_{2y}/F_{1y} ratio (where F_{1y} and F_{2y} denote the yield forces of X-shaped steel plates 1 and 2, respectively) increased. Similarly, in Group D-3F, altering the dimensions of X-shaped steel plate 3 led to an increase in the enclosed area of the third stage of the hysteresis curve with an increase in F_{3y}/F_{2y} (where F_{3y} represents the yield force of X-shaped steel plate 3).

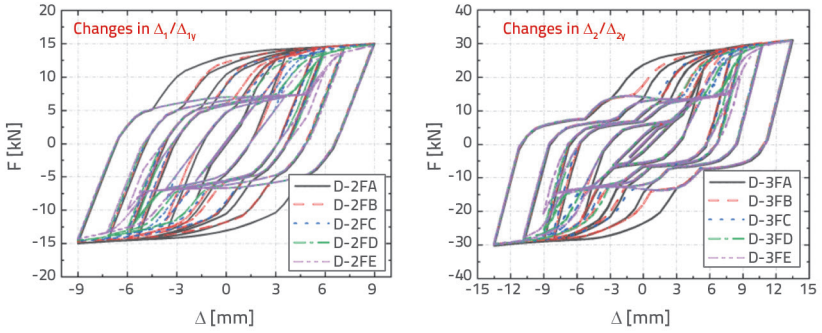

Figure 28. Hysteretic curve with changes in contact gap

The hysteresis curves for the damper under varying contact gap dimensions are shown in Figure 28 The hysteresis curves for Groups D-2 and D-3 exhibit pronounced multistage hysteretic characteristics. For Group D-2, when adjusting the dimension of the contact gap Δ_1, the second-stage characteristics of the hysteresis curve become increasingly distinct as the Δ_1/Δ_{1y} ratio (with Δ_{1y} denoting the yield displacement of X-shaped steel plate 1) increases; however, the enclosed area of the second-stage portion of the curve decreases accordingly. For Group D-3, as the contact gap Δ_2 is modified and the Δ_2/Δ_{2y} ratio (where Δ_{2y} represents the yield displacement of X-shaped steel plate 2) increases, the third-stage characteristics of the hysteresis curve become prominent, while the enclosed area of the third-stage segment diminishes progressively.

5.3. Skeleton line

Figure 29 shows the skeleton curves of the damper for various dimensions. Among these, the skeleton curve of Group D-1F exhibits typical bilinear characteristics, and its initial stiffness increases as the size of X-shaped Steel Plate 1 increases. In contrast, the skeleton curves of Groups D-2F and D-3F display

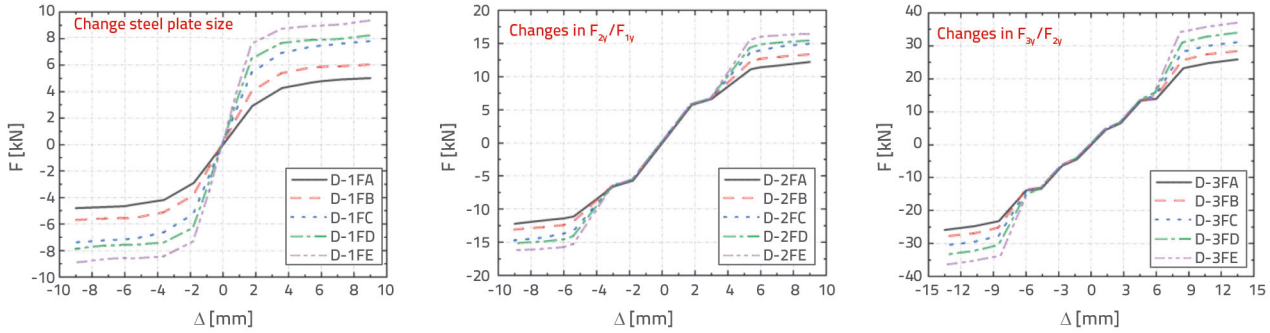

Figure 29. Skeleton line with changes in damper size

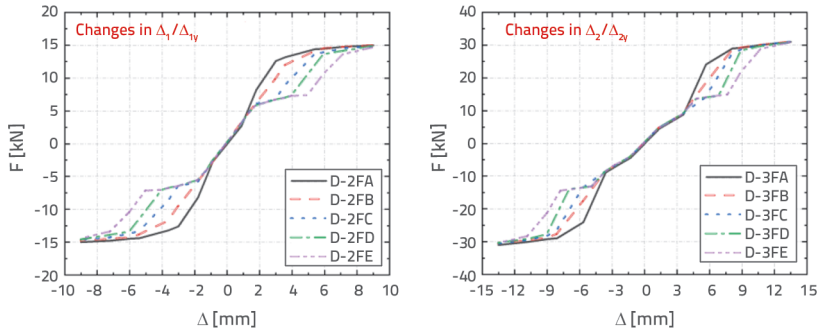

Figure 30. Skeleton line with changes in contact gap

distinct multistage hysteretic features. Specifically, in Group D-2F, when altering the size of X-shaped Steel Plate 2, the second-stage stiffness increased with an increase in the F_{2y}/F_{1y} ratio. For Group D-3F, as the size of the X-shaped Steel Plate 3 was adjusted, the third-stage stiffness demonstrated an upward trend with the increase in the F_{3y}/F_{2y} ratio.

Figure 30 illustrates the skeleton curve characteristics of a damper with varying contact gaps. For Group D-2, when adjusting the size of the contact gap Δ_1, the second-order characteristics of the system become more pronounced as the Δ_1/Δ_{1y} ratio increases, while the second-order stiffness exhibits a decreasing trend. In Group D-3, when adjusting the size of the contact gap Δ_2, the third-order characteristics grow more distinct with the increase in the Δ_2/Δ_{2y} ratio, though the third-order stiffness concurrently shows a declining trend.

5.4. Stiffness degradation curve

Figure 31 shows the stiffness degradation curves of the damper under dimensional variations. For Group D-1F, which was configured with only a single set of X-shaped steel plates as energy-dissipating components, the stiffness exhibited a sustained degradation trend throughout the energy-dissipation process. Notably, as the geometric dimensions of the X-shaped Steel Plate 1 increased, the initial stiffness of the damper improved significantly. In Group D-2F, the stiffness evolution during the initial stage of displacement loading (before the contact mechanism was triggered) aligned closely with that of Group D-1F. Once X-shaped Steel Plate 1 yields and enters the stiffness degradation phase, continued displacement growth activates the contact mechanism at gap 1. This triggers the engagement of X-shaped Steel Plate 2, which then forms a coordinated working mechanism with X-shaped Steel Plate 1. Consequently, the damping force increases significantly, accompanied by a notable stiffness enhancement, which is a distinct stiffness boost phenomenon. The magnitude of this stiffness improvement further increased with an increase in the F_{2y}/F_{1y} ratio. Group D-3F incorporates a dual-contact mechanism design. During progressive displacement loading, the stiffness variation upon triggering the contact mechanism at gap 1 mirrors was observed in Group D-2F. As the displacement continues

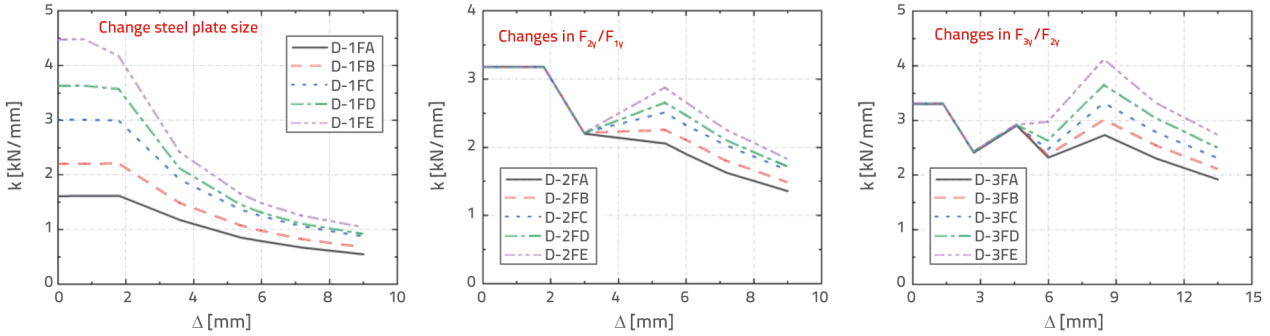

Figure 31. Stiffness degradation curve with changes in damper size

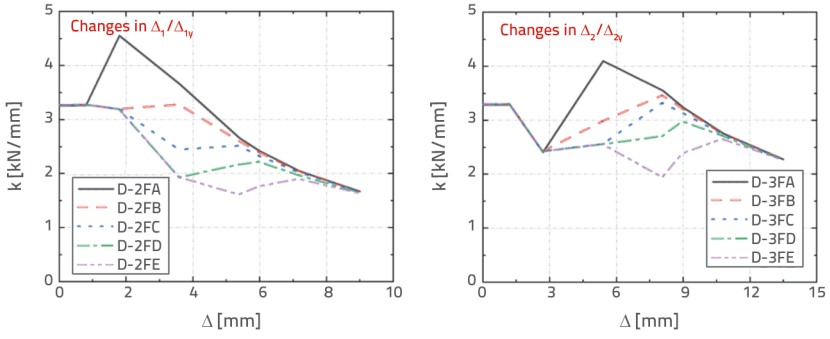

Figure 32. Stiffness degradation curve with changes in contact gap

5.5. Energy dissipation capacity

As shown in Figure 33, with the increase of displacement, the equivalent viscous damping coefficient ζ of specimens in Group D-1F exhibits distinct nonlinear growth characteristics as the X-shaped Steel Plate 1 undergoes elasto-plastic deformation, and this growth trend intensifies with the enlargement of the geometric dimensions of X-shaped Steel Plate 1. For Group D-2F specimens, the

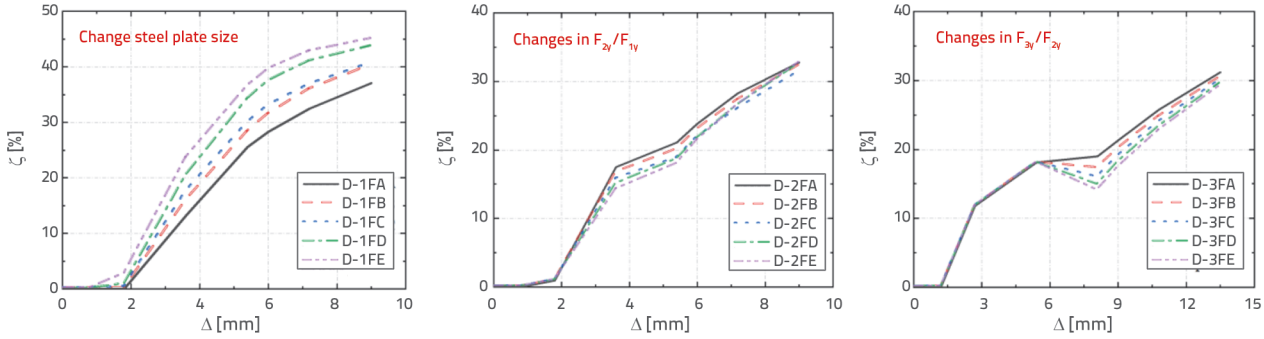

Figure 33. Equivalent viscous damping coefficient ζ curves with changes in damper size

to increase and reaches the activation threshold of the contact mechanism at gap 2, the X-shaped Steel Plate 3 is activated. This plate then collaborates with the centrally fixed X-shaped Steel Plate 1 and the already engaged X-shaped Steel Plate 2 to establish a three-body coordinated working mode. This cooperation leads to a recurrence of the damping force augmentation and further stiffness elevation, a second pronounced stiffness boost. The extent of this second stiffness enhancement increased similarly with an increase in the F_{3y}/F_{2y} ratio.

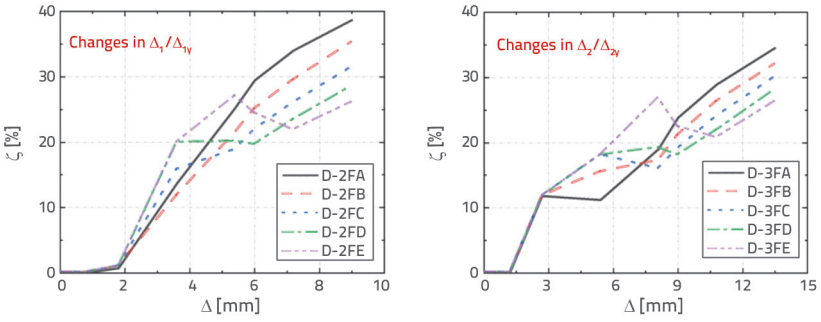

Figure 34. Equivalent viscous damping coefficient ζ curves with changes in contact gap

The stiffness degradation curves of the damper under various contact gap parameters are shown in Figure 32. For Group D-2, after the activation of the contact mechanism, X-shaped steel plate 2 at gap 1 was activated to cooperate with X-shaped steel plate 1 during operation. This results in an increase in damping force accompanied by stiffness enhancement; however, as the Δ_1/Δ_{1y} ratio increases, the second-stage stiffness enhancement diminishes. Group D-3 was equipped with a dual-contact mechanism. As the displacement continued to increase, the contact mechanisms at gaps 1 and 2 were sequentially activated, successively activating X-shaped steel plates 2 and 3. These plates then participated in the operation, together with the X-shaped steel plate 1 fixed in the middle. Nevertheless, as the Δ_2/Δ_{2y} ratio increases, the third-stage stiffness enhancement decreases progressively.

evolution of ζ follows a three-stage stepwise growth pattern: initial rapid ascent, mid-stage gradual transition, and late-stage accelerated increase. Notably, as the F_{2y}/F_{1y} ratio increases, the equivalent energy dissipation capacity of the system exhibits a regular attenuation trend. The ζ response of Group D-3F specimens also adheres to a fast-slow-fast three-stage growth model, where the slow-growth phase is predominantly concentrated in the second-stage displacement interval. With an increase in the F_{3y}/F_{2y} ratio, the energy dissipation capacity of the specimen in the third-stage displacement application range exhibited progressive enhancement characteristics.

As shown in Figure 34, with the increase of loading displacement, the equivalent viscous damping coefficient ζ of Group D-2 exhibits a characteristic pattern of rapid initial growth followed by a slight subsequent decline. This behavioural trait becomes more pronounced as the $\Delta_1/$

Δ_{1y} ratio increases. For Group D-3, its ζ variation pattern is similar to that of Group D-2, also showing a rapid increase initially, followed by a brief decline. This was primarily because the initially engaged X-shaped steel plate 2 remained in the elastic deformation stage during early loading and failed to effectively contribute to energy dissipation. As displacement continues to increase and X-shaped steel plate 2 transitions into elastoplastic deformation, ζ does rebound temporarily. However, since X-shaped steel plate 3, upon initial engagement, still remains in the elastic deformation state, the phased suppression effect of its hysteresis loop area leads to a secondary decline in ζ. Only when X-shaped steel plate 3 entered the elastoplastic deformation stage did the damping coefficient achieve sustained growth. Notably, this characteristic becomes more evident as the Δ_2/Δ_{2y} ratio increases.

The above analyses of damper tests and numerical simulations reveal the following key findings. For the first-order D-1 series dampers, as the geometric dimensions of the X-shaped steel plates increase, both their energy dissipation capacity and initial stiffness exhibit an upward trend, although the post-yield stiffness declines rapidly. For the second-order D-2 series dampers, the energy dissipation capacity generally decreased slightly with increasing yield strength ratio, F_{2y}/F_{1y}. When F_{2y}/F_{1y} exceeds 1, the participation of the X-shaped steel plate 2 after the yielding of plate 1 can restore or even exceed the initial stiffness of the damper. Additionally, as Δ_1/Δ_{1y} increases, the energy dissipation capacity drops significantly upon the engagement of plate 2, and the stiffness superposition effect becomes weaker than the initial state. However, when $\Delta_1/\Delta_{1y}<1.5$, both the stiffness superposition effect and energy dissipation capacity perform better. For the adaptive D-3 series dampers, the energy dissipation capacity showed a marginal overall decrease with increasing yield strength ratio, F_{3y}/F_{2y}. When F_{3y}/F_{2y} exceeds 2, the participation of the X-shaped steel plate 3 after the yielding of plates 1 and 2 restores the initial stiffness of the damper to or beyond its original level. Concurrently, as Δ_2/Δ_{2y} increases, the energy dissipation capacity declines notably upon the engagement of plate 3, and the stiffness superposition effect weakens relative to the initial state. Nevertheless, when $\Delta_2/\Delta_{2y}<3$, both the stiffness superposition effect and energy dissipation capacity demonstrate favourable performance.

6. Conclusions

Based on a combined research methodology integrating low-cycle repeated pseudostatic tests and finite element numerical simulations, this study conducted a systematic investigation of the seismic performance of a novel adaptive damper. The key conclusions are summarised as follows:

- The adaptive damper achieves multistage energy dissipation and stiffness superposition through the graded bending deformation of three-stage X-shaped steel plates. The contact gap activation mechanism enables the damping force to increase progressively with displacement, resulting in a hysteretic curve characterised by multipeak features.
- The stiffness degradation curves reveal that after an initial reduction in stiffness, the adaptive damper undergoes stiffness recovery following the activation of the contact mechanism, resulting in dynamic stiffness matching. This feature effectively addresses the issue of continuous stiffness degradation in conventional dampers.
- The equivalent viscous damping coefficient of the adaptive damper peaks at the maximum displacement. However, owing to the influence of the elastic deformation stage of the subsequently engaged X-shaped steel plates, a temporary suppression of the energy dissipation capacity occurs. The optimisation of the geometric parameters of X-shaped steel plates can mitigate the attenuation of the energy dissipation efficiency.
- The finite-element numerical simulation results aligned closely with the experimental curves, validating the effectiveness of the adaptive damper in multistage energy dissipation and stiffness regulation. These findings provide a robust scientific basis for the application of the proposed damper as a displacement-based energy-dissipating support for the seismic design of frame structures.

Acknowledgements

The Research Fund Project for the Academician Workstation of the China Academy of Building Science (No.20220122330730021) provided financial support for this study, which is gratefully acknowledged. Any opinions, findings, conclusions, or recommendations expressed in this study are those of the authors and do not necessarily reflect the views of the sponsors.

REFERENCES

[1] Shmerling, A., Levy, R., Reinhorn, A.M.: Seismic retrofit of frame structures using passive systems based on optimal control, Structural Control and Health Monitoring, 25 (2018) 1, pp. e2038, https://doi.org/10.1002/stc.2038

[2] Xue, Q., Wu, C.W., Chen, C.C., et al.: Post-earthquake loss assessment based on structural component damage inspection for residential RC buildings, Engineering Structures, 31 (2009) 12, pp. 2947-2953, https://doi.org/10.1016/j.engstruct.2009.07.022

[3] Jaisee, S., Yue, F., Ooi, Y.H.: A state-of-the-art review on passive friction dampers and their applications, Engineering Structures, 235, (2021), Paper 112022, https://doi.org/10.1016/j.engstruct.2021.112022

[4] Symans, M.D., Charney, F.A., Whittaker, A.S. et al.: Energy dissipation systems for seismic applications: current practice and recent developments, Journal of structural engineering, 134 (2008) 1, pp. 3-21, https://doi.org/10.1061/(ASCE)0733-9445(2008)134:1(3)

[5] Kelly, J.M., Skinner, R.I., Heine, A.J.. Mechanisms of energy absorption in special devices for use in earthquake resistant structures, Bulletin of the New Zealand Society for Earthquake Engineering, 5 (1972) 3, pp. 63-88, https://doi.org/10.5459/bnzsee.5.3.63-88

[6] Farajiani, F., Elyasigorji, F., Elyasigorji, S. et al.: Effect of U-shaped metallic dampers on the seismic performance of steel structures based on endurance-time analysis, Buildings, 14 (2024) 5, Paper 1368, https://doi.org/10.3390/buildings14051368

[7] Kandemir, E.C., Jankowski, R.: Effect of soil on the capacity of viscous dampers between adjacent buildings, Gradevinar, 75 (2023), pp. 329-342, https://doi.org/10.14256/JCE.3597.2022

[8] Ghasemi Jouneghani, H., Haghollahi, A., Mortazavi, M.: Pushover analysis for estimating seismic demand of elliptic braced moment resisting frames, Građevinar, 74 (2022) 11, pp. 941-955, https://doi.org/10.14256/JCE.2311.2017

[9] Nižić, A., Meštrović, D.: Seismic dampers in engineering structures, Građevinar, 63 (2011) 07, pp. 661-667.

[10] Zhou, Z., Chen, Y., Yam, M.C. et al.: Experimental investigation of a high strength steel frame with curved knee braces subjected to extreme earthquakes, Thin-Walled Structures, 185 (2023). Paper 110596, https://doi.org/10.1016/j.tws.2023.110596

[11] Ke, K., Chen, Y., Zhou, X. et al.: Experimental and numerical study of a brace-type hybrid damper with steel slit plates enhanced by friction mechanism, Thin-Walled Structures, 182 (2023), Paper 110249, https://doi.org/10.1016/j.tws.2022.110249

[12] Hu, S., Wang, W., Lu, Y.: Explainable machine learning models for probabilistic buckling stress prediction of steel shear panel dampers, Engineering Structures, 288 (2023). Paper 116235, https://doi.org/10.1016/j.engstruct.2023.116235

[13] Chen, Y., Chen, C., Jiang, H., et al.: Study of an innovative graded yield metal damper, Journal of Constructional Steel Research, 160 (2019), pp. 240-254, https://doi.org/10.1016/j.jcsr.2019.05.028

[14] Bergman, D.M., Goel, S.C.: Evaluation of cyclic experimenting of steel plate devices for added damping and stiffness, Report No. UMCE87-10, The University of Michigan, Ann Arbor, MI, USA, 1987.

[15] Martinez-Romero, E.: Experiences on the use of supplementary energy dissipators on building structures, Earthquake spectra, 9 (1993) 3, pp. 581-625, https://doi.org/10,1193/1,1585731

[16] Perry, C.L., Fierro, E.A., Sedarat, H., et al.: Seismic upgrade in San Francisco using energy dissipation devices, Earthquake Spectra, 9 (1993) 3, pp. 559-579, https://doi.org/10,1193/1,1585730

[17] Xia, C., Hanson, R.D.: Influence of ADAS element parameters on building seismic response, Journal of Structural Engineering, 118 (1992) 7, pp. 1903-1918, https://doi.org/10.1061/(asce)0733-9445(1992)118:7(1903)

[18] Tsai, K.C., Chen, H.W., Hong, C.P., et al.: Design of steel triangular plate energy absorbers for seismic-resistant construction, Earthquake spectra, 9 (1993) 3, pp. 505-528, https://doi.org/10,1193/1,1585727

[19] Oh, S.H., Kim, Y.J., Ryu, H.S.: Seismic performance of steel structures with slit dampers, Engineering structures, 31 (2009) 9, pp. 1997-2008, https://doi.org/10.1016/j.engstruct.2009.03.003

[20] Balendra, T., Yu, C.H., Lee, F.L.: An economical structural system for wind and earthquake loads, Engineering Structures, 23 (2001) 5, pp. 491-501, https://doi.org/10.1016/s0141-0296(00)00061-4

[21] Sun, J., Pan, P., Wang, H.: Development and experimental validation of an assembled steel double-stage yield buckling restrained brace, Journal of Constructional Steel Research, 145 (2018), pp. 330-340, https://doi.org/10.1016/j.jcsr.2018.03.003

[22] Cheraghi, A., Zahrai, S.M.: Cyclic experimenting of multilevel pipe in pipe damper, Journal of Earthquake Engineering, 23 (2019) 10, pp. 1695-1718, https://doi.org/10.1080/13632469.2017.1387191

[23] Chen, Y., Chen, C., Jiang, H., et al.: Study of an innovative graded yield metal damper, Journal of Constructional Steel Research, 160 (2019), pp. 240-254, https://doi.org/10.1016/j.jcsr.2019.05.028

[24] Li, G.Q., Sun, Y.Z., Jiang, J., et al.: Experimental study on two-level yielding buckling-restrained braces, Journal of Constructional Steel Research, 159 (2019), pp. 260-269, https://doi.org/10.1016/j.jcsr.2019.04.042

[25] Ristic, J., Behrami, R., Brujić, Z., Ristic, D., Hristovski, V.: Method for upgrading isolated bridges with novel V gaped devices: Seismic experiments of models, GRAĐEVINAR, 76 (2024) 9, pp. 789-802, https://doi.org/https://doi.org/10.14256/JCE.3937.2024

[26] Ristic, J., Ristic, D., Hristovski, V.: Upgrading of isolated bridges with uniform gapped HS devices: Seismic experiments, GRAĐEVINAR, 74 (2022) 12, pp. 1047-1058, https://doi.org/https://doi.org/10.14256/JCE.3580.2022

[27] Zhang, S., Zhang, C., Ju, X., Xiong, Y.: Study on seismic dissipation mechanism of inter-story isolation structure based on phase, GRAĐEVINAR, 75 (2023) 10, pp. 969-978, https://doi.org/https://doi.org/10.14256/JCE.3643.2022

[28] Dang, B., Li, T., Wang, S., Zhan, M.: Design method and engineering application of shear wall with friction energy dissipation damper, GRAĐEVINAR, 74 (2022) 4, pp. 277-289, https://doi.org/https://doi.org/10.14256/JCE.2742.2019

[29] JGJ101-2015.: Specification for seismic experiment of building (in Chinese). Ministry of Housing and Urban-Rural Construction, 2015.